Electronic Supplementary Material (ESI) for ChemComm.

Single-Molecule Conductance in a Unique *Cross*-Conjugated Tetra(Aminoaryl)-Ethene

Samara Medina Rivero, Paloma García Arroyo, Liang Li, Suman Gunasekaran, Thijs Stuyver, María José Mancheño, Mercedes Alonso*, Latha Venkataraman*, José L. Segura*, Juan Casado[a]*

SUPPORTING INFORMATION

TABLE OF CONTENTS

All air and moisture sensitive reactions were carried out under an inert atmosphere of argon. Purification by column chromatography was carried out on silica gel (flash column, SiO_2 40-63 µm). Thin-layer chromatography (TLC) was carried out on commercially available precoated plates (silica 60).

^1H NMR and ^{13}C NMR spectra were recorded on a 300 MHz spectrometer. Chemical shifts are reported in ppm and referenced to the residual non-deuterated solvent frequencies ($CDCl_3$: δ 7.26 ppm for ^1H, 77 .0 ppm for ^{13}C). Mass spectra were recorded by means of MALDI-TOF. Solids were analyzed on a diamond plate (ATR) or as films on sodium chloride.

II. Synthetic Procedures

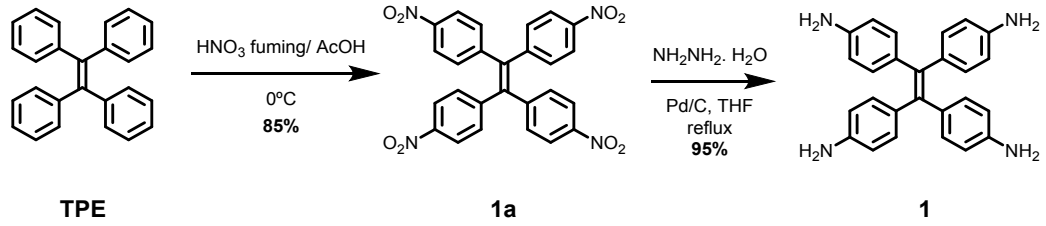

Scheme S1. Synthesis of molecule **1**.

Tetrakis(4-nitrophenyl)ethylene (1a)

1a was synthesized by following a previously reported procedure.[1] In an ice bath, acetic acid (13 mL, 0.2 mmol) and fuming nitric acid (13 mL, 0.3 mmol) were added to a 100 mL two neck round bottom flask. **TPE** (1,5 g, 4,6 mmol) was slowly added in small portions. Then the solution was warmed to room temperature and stirred for 3h. The reaction mixture was poured into ice water (100 mL) and the yellow precipitated was collected by filtration, washed with an excess of water, and air dried, affording **1a** as a light yellow powder (2.1 g, 85%). ^1H NMR (300 MHz, $CDCl_3$, 298 K): δ = 8.08 (d, *J* = 8.90 Hz, 8H), 7.19 (d, *J* = 8.90 Hz, 8H).

Tetrakis(4-aminophenyl)ethylene (1)

1 was synthesized by following a previously reported procedure.[1] To a solution of tetrakis(4-nitrophenyl)ethylene **1a** (400 mg, 0.78 mmol) in dry THF (5 mL) under argon atmosphere,

palladium on carbon (wt 10 % Pd, 83 mg) and $NH_2NH_2 \cdot H_2O$ (5.8 mL, 93 mmol) were added. The solution was refluxed for 48 h. After that, the reaction mixture was cooled down to room temperature, and the insoluble residues were filtered off. The solvent of the filtrate was removed under reduced pressure to afford as a brown solid (291 mg, 95%). ^{1}H NMR (300 MHz, DMSO-d_6, 298 K): δ = 6.57 (d, *J* = 8.50 Hz, 8H), 6.26 (d, *J* = 8.50 Hz, 8H), 4.84 (s, 8H).

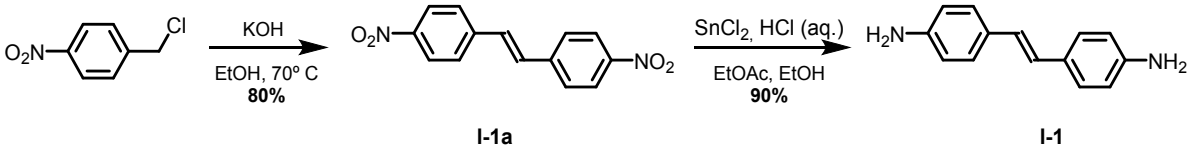

I-1a **I-1**

Scheme S2. Synthesis of the *trans* model compound.

4,4′-Dinitro-*trans*-stilbene (I-1a)

I-1a was synthesized by following a previously reported procedure.[2] Nitrobenzyl chloride (2.5 g, 14.6 mmol) was dissolved in 8 mL of heated ethanol. Then a solution of KOH (1 g, 17.8 mmol) in a mixture of water (0,75 ml) and ethanol (3 mL) was added dropwise at room temperature. The resulting reaction mixture was stirred for 2 h at 70 °C. After the reaction time, it was cooled and filtered. The residue was washed with an excess of ethanol, affording **I-1a** as yellow needles (3 g, 80%). ^{1}H NMR (CDCl3, 300 MHz, ppm): δ = 8.28 (d, *J* = 8.90 Hz, 4H), 7.94 (d, *J* = 8.90 Hz, 4H) 7.70 (s, 2H).

4,4′-Diamino-*trans*-stilbene (I-1)

I-1 was synthesized by following a previously reported procedure.[3] To a suspension of **I-1a** (150 mg, 0.55 mmol) in a mixture of solvents (EtOH/EtOAc, 10 ml/ 10 ml)) was added concentrated HCl (aq) (5 mL) under stirring at room temperature. Subsequently, $SnCl_2$ $2H_2O$ (1.25 g, 5.5 mmol) was added, and the mixture was heated to 80 ºC for 5 h. After cooling to room temperature, the reaction mixture was filtered. The filtrate was concentrated and washed with saturated aqueous NaCl and dried over $MgSO_4$. The solvent was removed under reduced pressure to afford **I-1** as a brownish solid (112 mg, 96.0%). ^{1}H NMR (CDCl3, 300 MHz, ppm): δ = 7.29 (d, *J* = 8.90 Hz, 4H), 6.84 (s, 2H) 6.66 (d, *J* = 8.90 Hz, 4H) 3.69 (broad s, 4H).

1,1-bis(4-aminophenyl)ethylene (c-1)

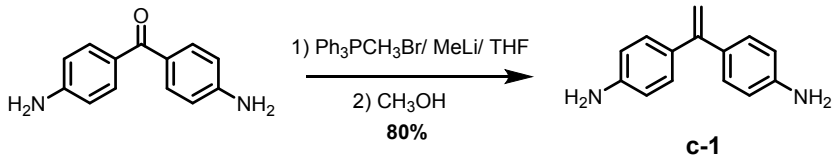

Scheme S3. Synthesis of the *cross* model compound.

c-1 was synthesized by following a previously reported procedure.[4] Methyltriphenylphosphonium bromide (404 mg, 1.13 mmol) was disolved in freshly distilled THF (5 mL) under Ar atmosphere.The mixture was degassed with Ar for 15 min. Methyllithium (0.71 mL of a 1.6 mol L^{-1} solution in diethyl ether, 1.13 mol) was added dropwise to the reaction flask at 0 ºC, whereupon the reaction mixture turned yellowish. After stirring for 4 h at room temperature, the resulting phosphorus ylide was transferred via a cannula into a solution of 4,4′-diaminobenzophenone (200 mg, 0.94 mmol) in dry THF (5 mL) at 0 ºC. The reaction mixture was stirred under reflux for 12 h. The resultant brown solution was quenched with methanol (0.2 mL). The formed triphenylphosphine oxidesalt was removed by vacuum filtration. The filtrate was concentrated and the crude product was purified by silica gel column chromatography using hexane/ethylacetate (20:80, v/v). Recrystallization of the solid from 80% aqueous ethanol solution afforded pure **c-1** as pale yellow crytals (159 mg, 80%). ^{1}H NMR (300 MHz, $CDCl_3$, 298 K): δ = 7.16 (d, *J* = 8.61 Hz, 4H), 6.63 (d, *J* = 8.61 Hz, 4H), 5.19 (s, 2H), 3.69 (broad s, 4H).

III. NMR spectra

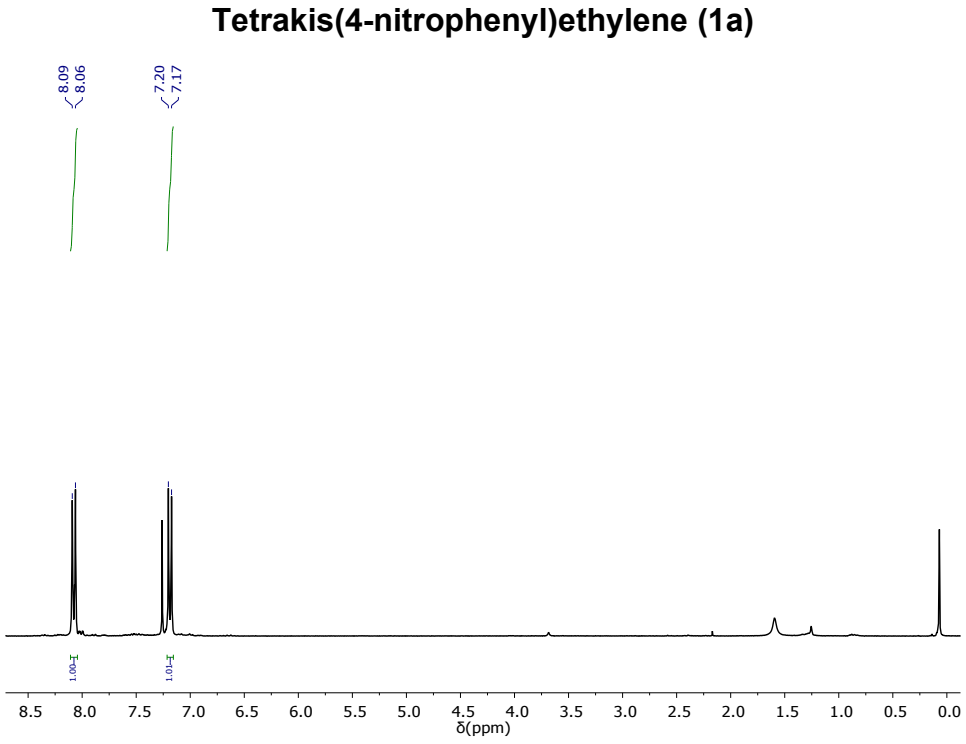

Figure S1. ^{1}H-NMR spectrum of **1a** in $CDCl_3$ (300 MHz).

Tetrakis(4-aminophenyl)ethylene (1a)

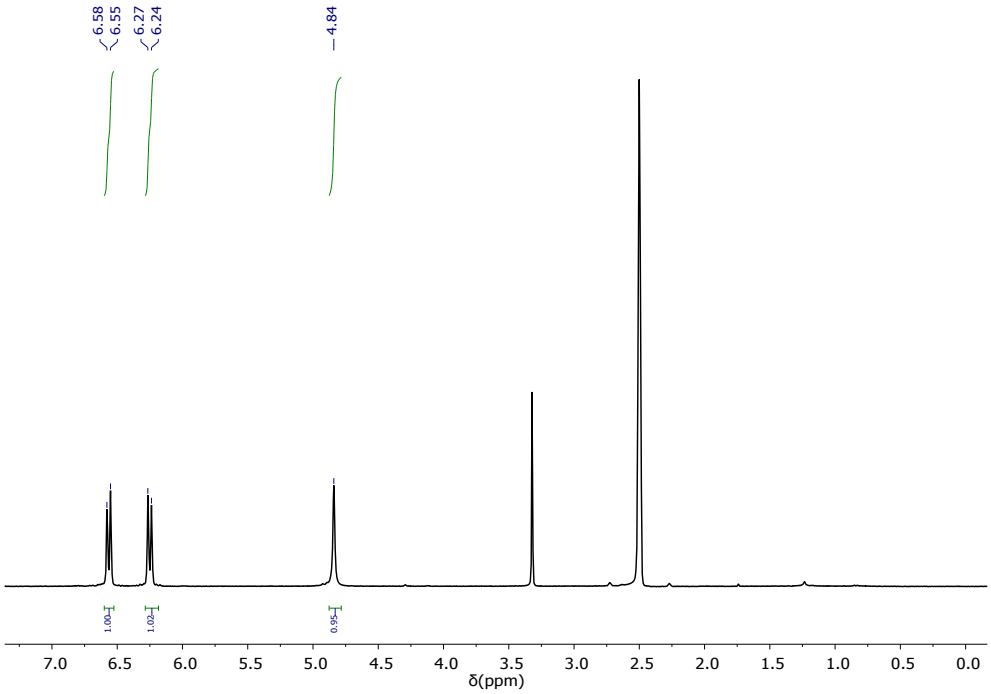

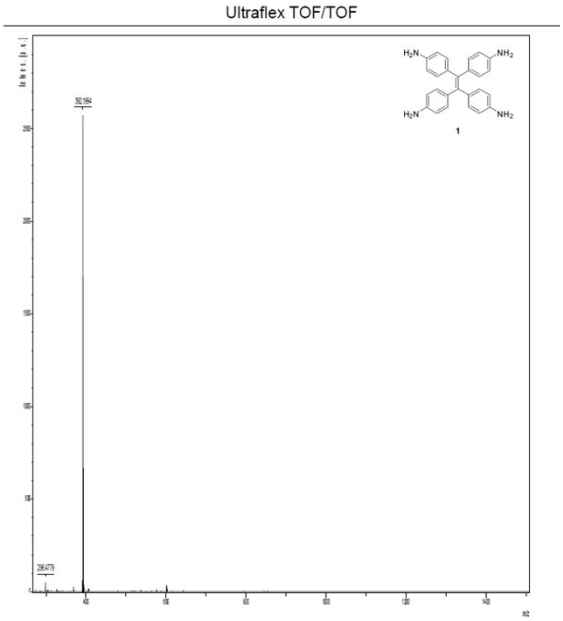

Ultraflex TOF/TOF

m/z	Rel. Intens.	Res.
298.4779	2	2217
391.1858	2	3037
392.1994	100	3097
393.2048	26	3098
394.2137	1	3084

Figure S2. ^{1}H-NMR spectrum (top) of **1** in DMSO-d_6 (300 MHz) together with its mass spectrum (bottom).

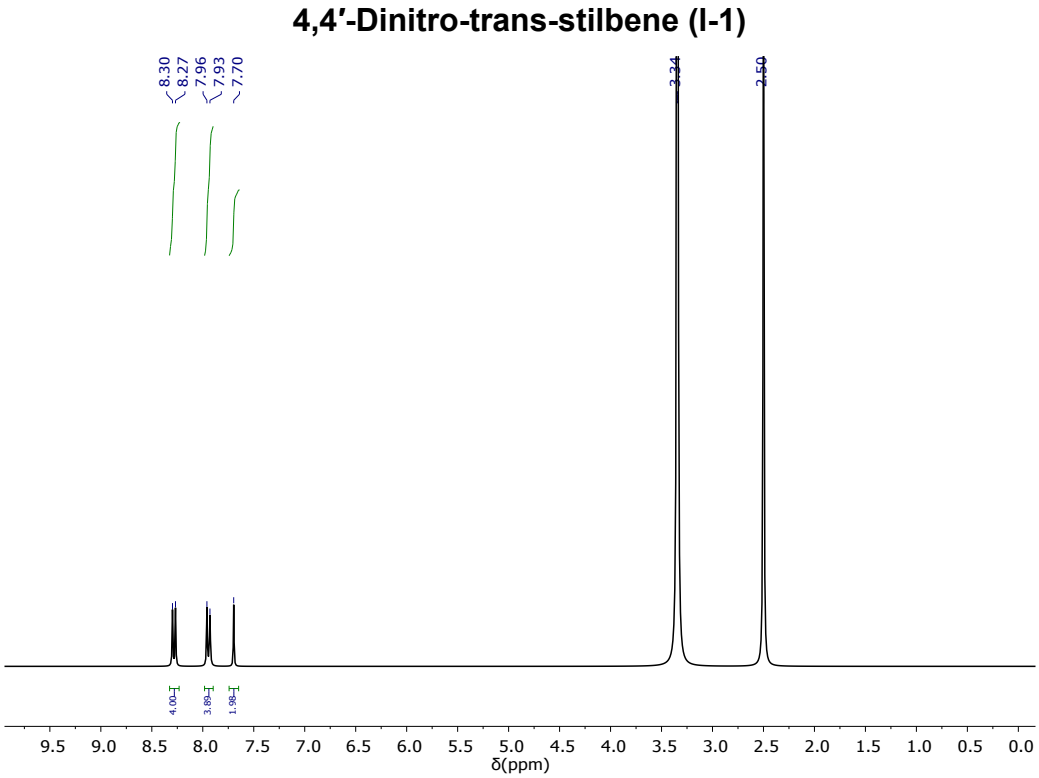

Figure S3. ^{1}H-NMR spectrum (top) of **I-1** in DMSO-d_6 (300 MHz)

4,4′-Diamino-trans-stilbene (I-1)

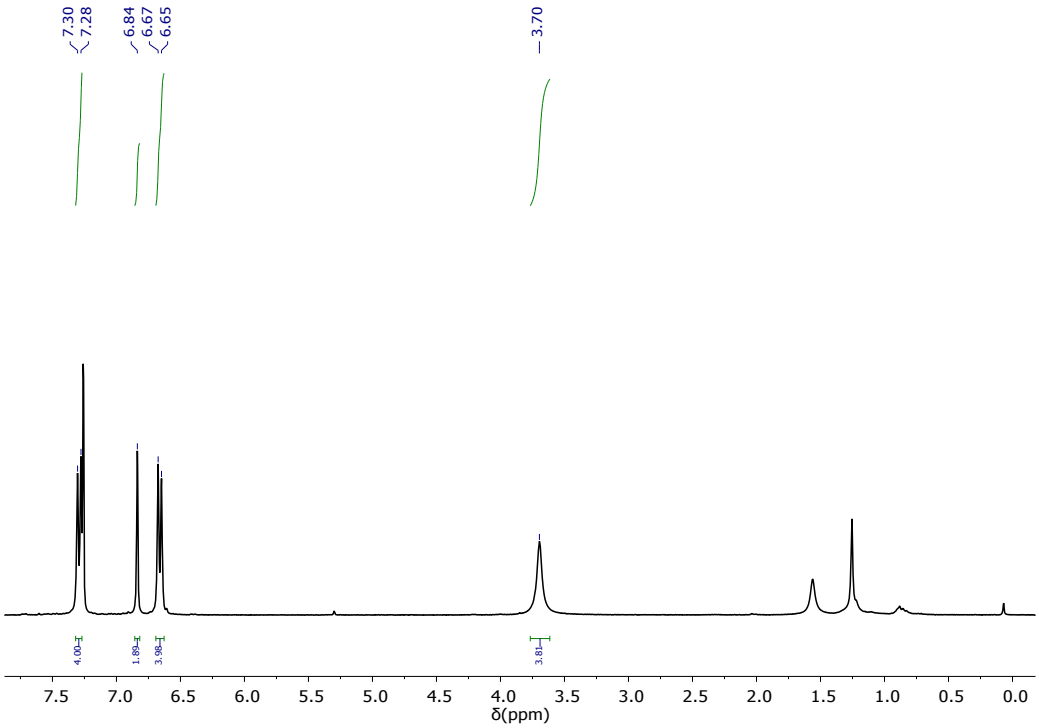

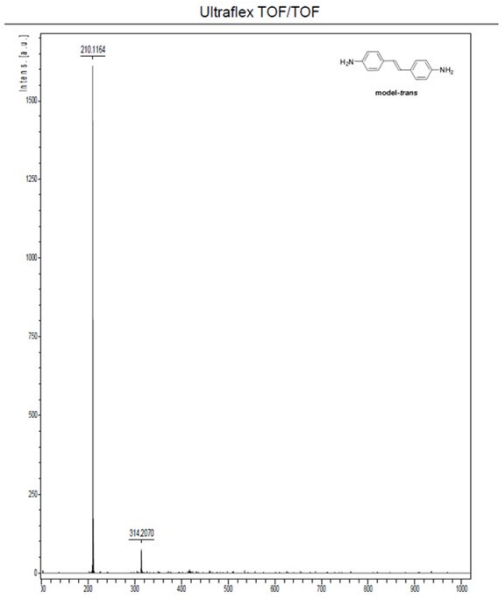

Ultraflex TOF/TOF

m/z	Rel. Intens.	Res.
209.1113	1	8792
210.1164	100	6583
211.1210	8	8203
313.2041	1	19328
314.2070	5	11678

Figure S4. ^{1}H-NMR spectrum (top) of **I-1** in $CDCl_3$ (300 MHz) together with its mass spectrum (bottom).

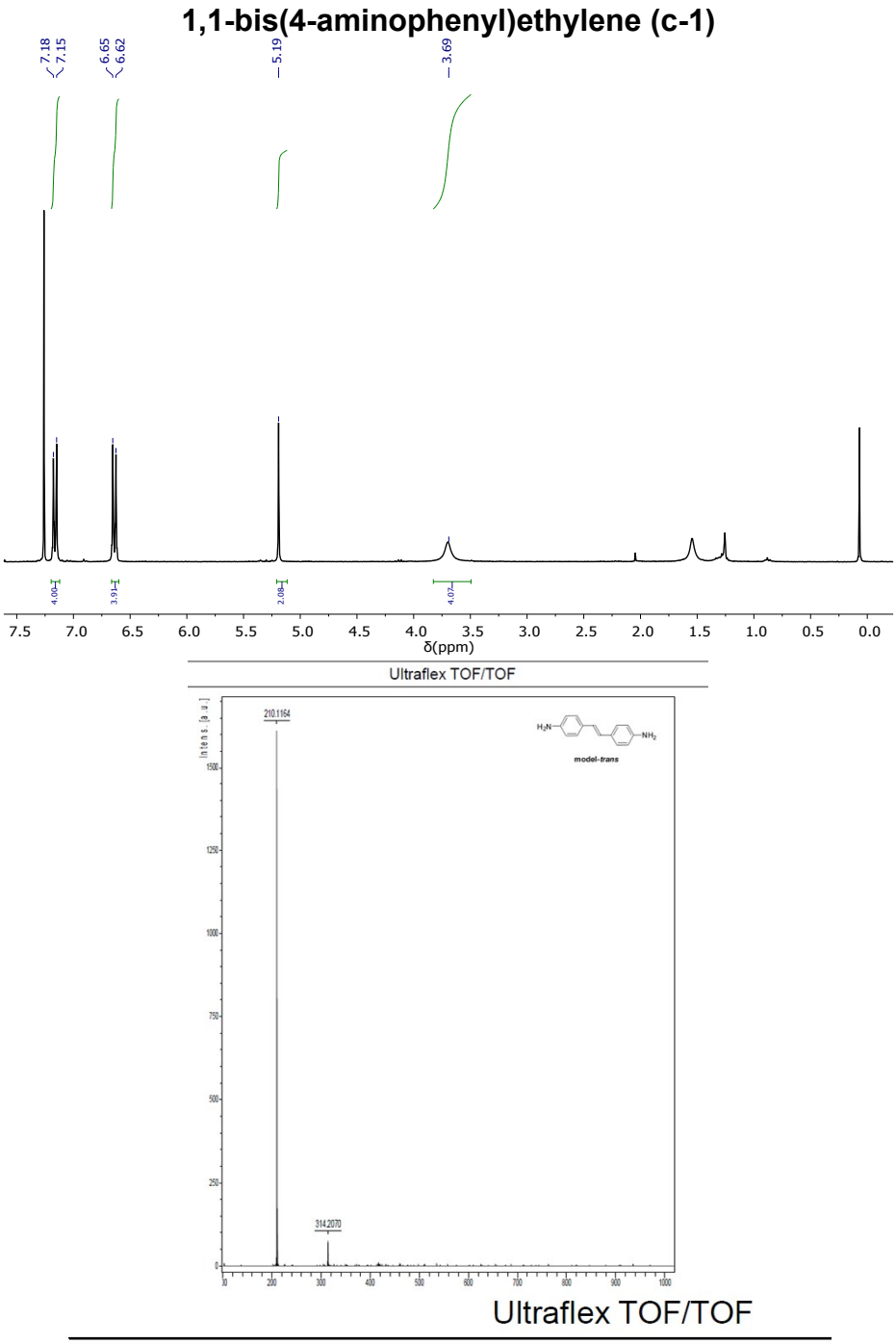

m/z	Rel. Intens.	Res.
209.1113	1	8792
210.1164	100	6583
211.1210	8	8203
313.2041	1	19328
314.2070	5	11678

Figure S5. ^{1}H-NMR spectrum (top) of **c-1** in $CDCl_3$ (300 MHz) together with its mass spectrum (bottom).

.

IV. Spectrochemical Titration and DFT Calculations

Titration experiments have been conducted in dichloromethane at room temperature by progressive addition of trifluoroacetic acid (TFA) to a 10^{-6} M solution of **1**. In situ UV-Vis spectrochemical studies were conducted on the Varian Cary 5000 UV-Vis-NIR Spectrophotometer.

DFT calculations were performed with the Gaussian16 suite of programs.[5] Molecular geometry optimizations were performed with the B3LYP functional and the 6-31G** standard basis set[6,7] and with the Handy and coworkers' long-range-corrected version of B3LYP using the Coulomb-attenuating method (CAM-B3LYP)[8]. To simulate the solvent environment, a polarizable continuum model (PCM) was employed[9-12]. This model places the solute molecule into a size-adapted cavity formed from overlapping atom-centered van der Waals spheres, while the solvent is assimilated to a continuum characterized by its dielectric constant (8.93 for dichloromethane). Energy optimizations were performed by allowing all geometric parameters to vary independently. The optimum energy structures were found to be a true minimum in the ground state potential energy surface. Vertical transition energies were computed with the time-dependent version of DFT (TDDFT) [13, 14].

Titration of **1** with trifluoroacetic acid (TFA) has been afforded and protonation proceeds with the generation of one distinctive UV-Vis absorption spectrum which, after clearance of the neutral features at 274/340 nm, is featured by the growing of a couple of bands at 310-317 nm and another at 436 nm. TD-DFT/B3LYP/6-31G** calculations in CH_2Cl_2 have been carried out for the different bis-protonated species of **1.** It is found that the bis-protonation occupying the two distal positions of the linear *trans*-conjugated path gives rise to a main band at 300 nm accompanied by another transition at 442 nm, in very nice agreement with the two bands observed experimentally. Alternatively, if bis-protonation of **1** is occupying the *cross*-conjugation positions, two theoretical excitations at 363 and 421 nm are predicted, while if the dication is occupying the *cis*-disposition, two transitions at 358 and 459 nm are revealed. These two *cross* and *cis* theoretical spectra clearly differ from the experimental one in the intensity ratio.

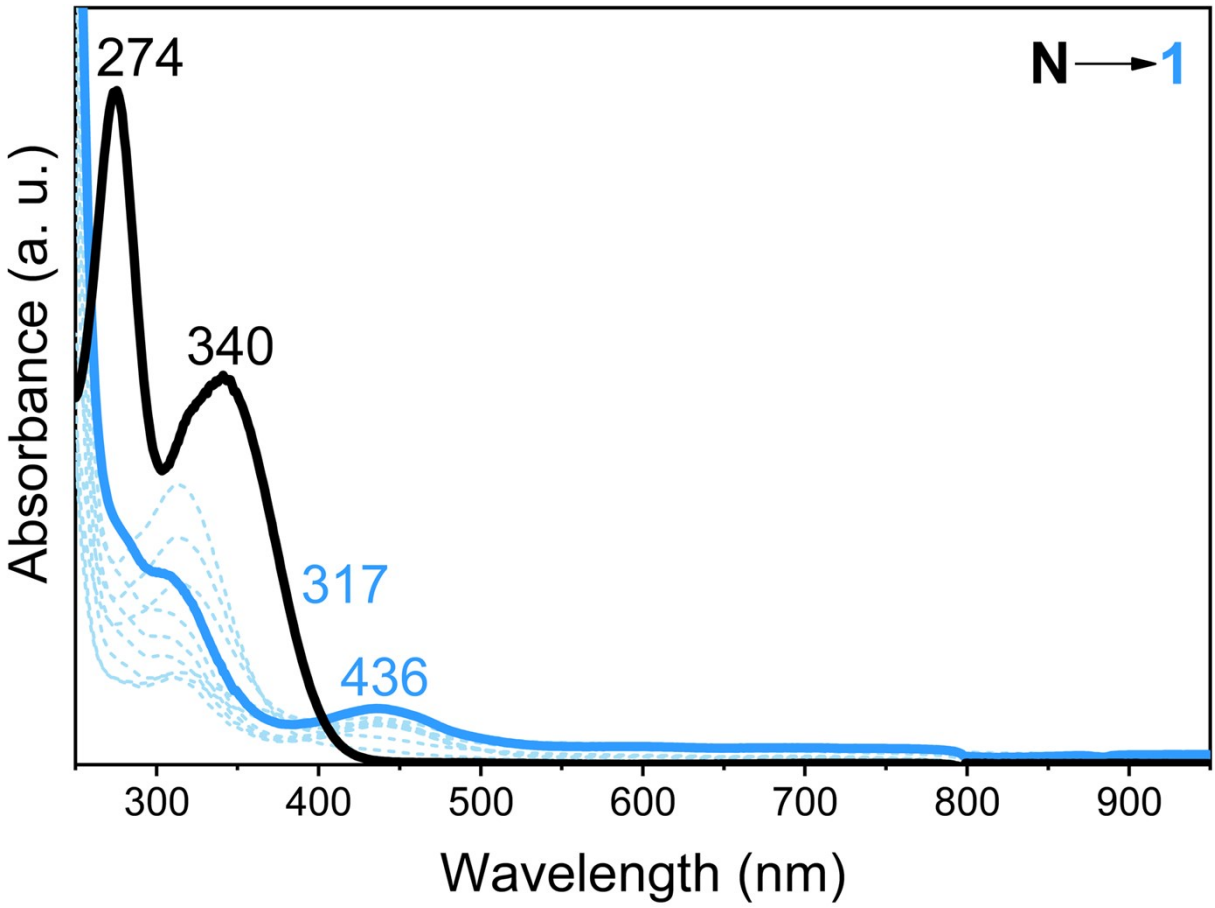

Figure S6. UV-Vis spectrochemical titration with TFA of **1** in CH_2Cl_2 at 10^{-6} M at room temperature. Black line corresponds to the neutral species and blue line corresponds to the completely formed first protonated species. Dashed lines correspond to intermediate spectra between the former species in the titration process.

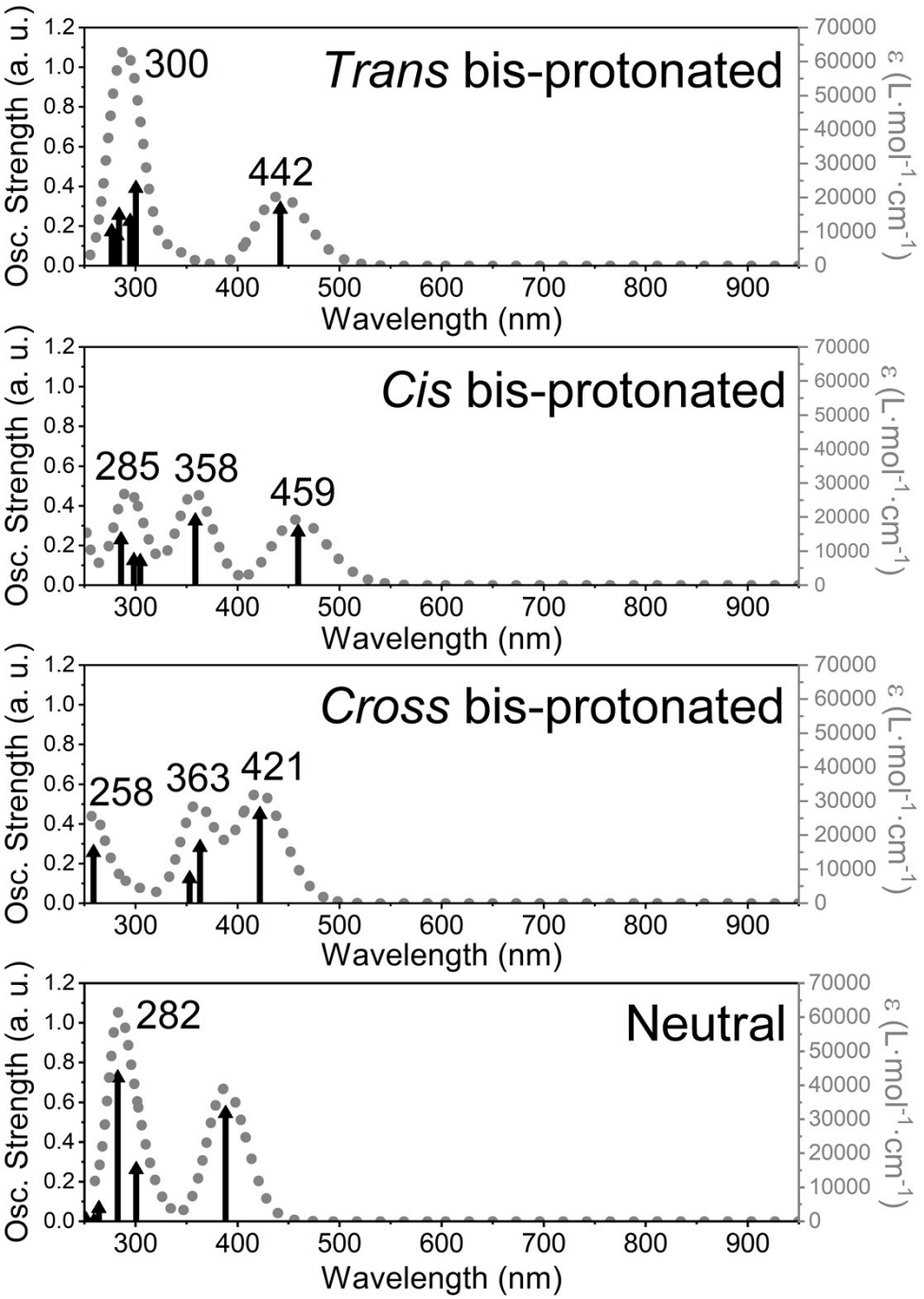

Figure S7. TD-DFT/B3LYP/6-31G** calculations in the framework of PCM model in CH_2Cl_2 of neutral and protonated species of **1**. From bottom to top: Neutral **1**; bisprotonated **1** in *cross* position; bisprotonated **1** in *cis* position; and bisprotonated **1** in *trans* position.

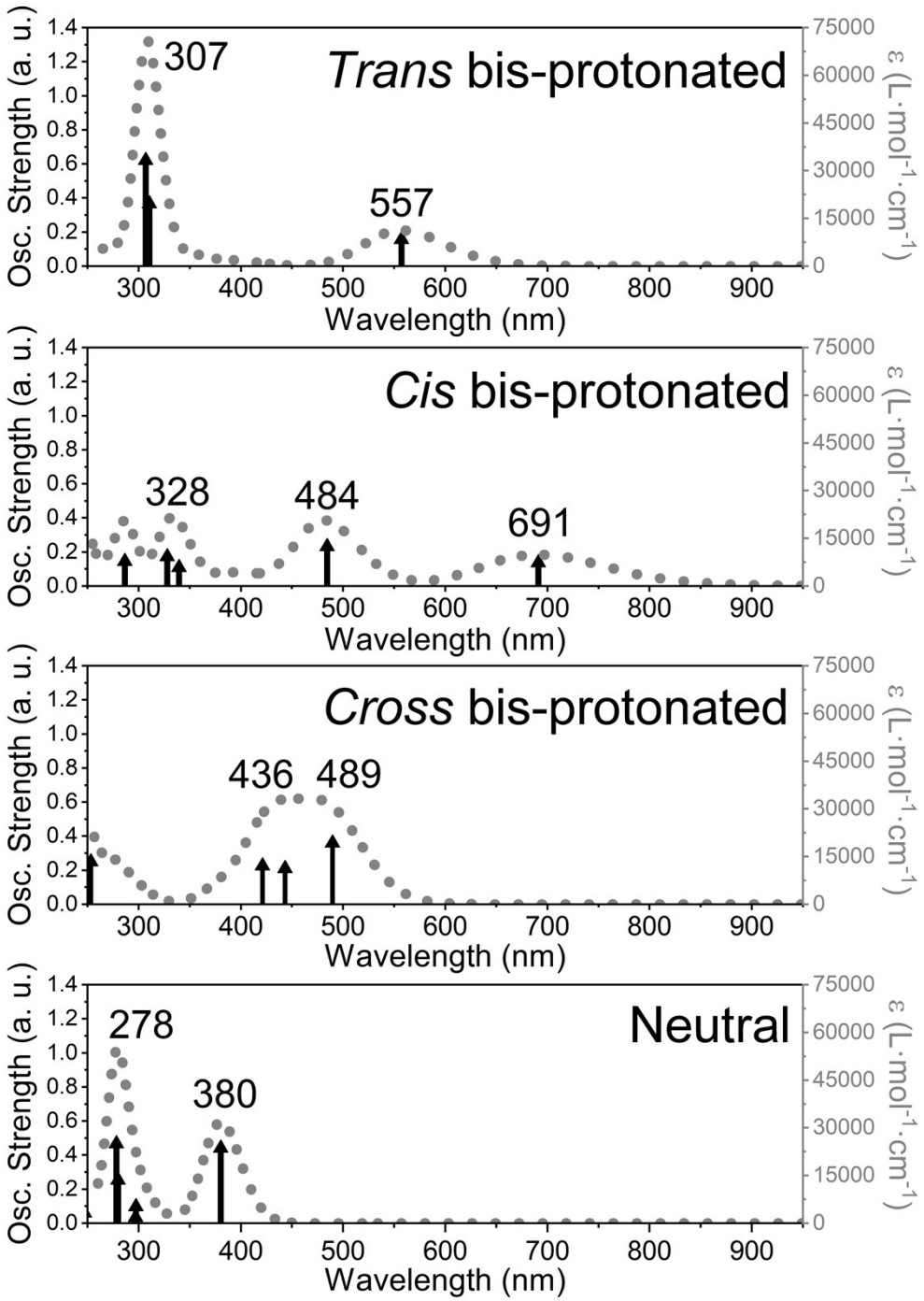

Figure S8. TD-DFT/B3LYP/6-31G** calculations in vacuum of neutral and protonated species of **1**. From bottom to top: Neutral **1**; bisprotonated **1** in *cross* position; bisprotonated **1** in *cis* position; and bisprotonated **1** in *trans* position.

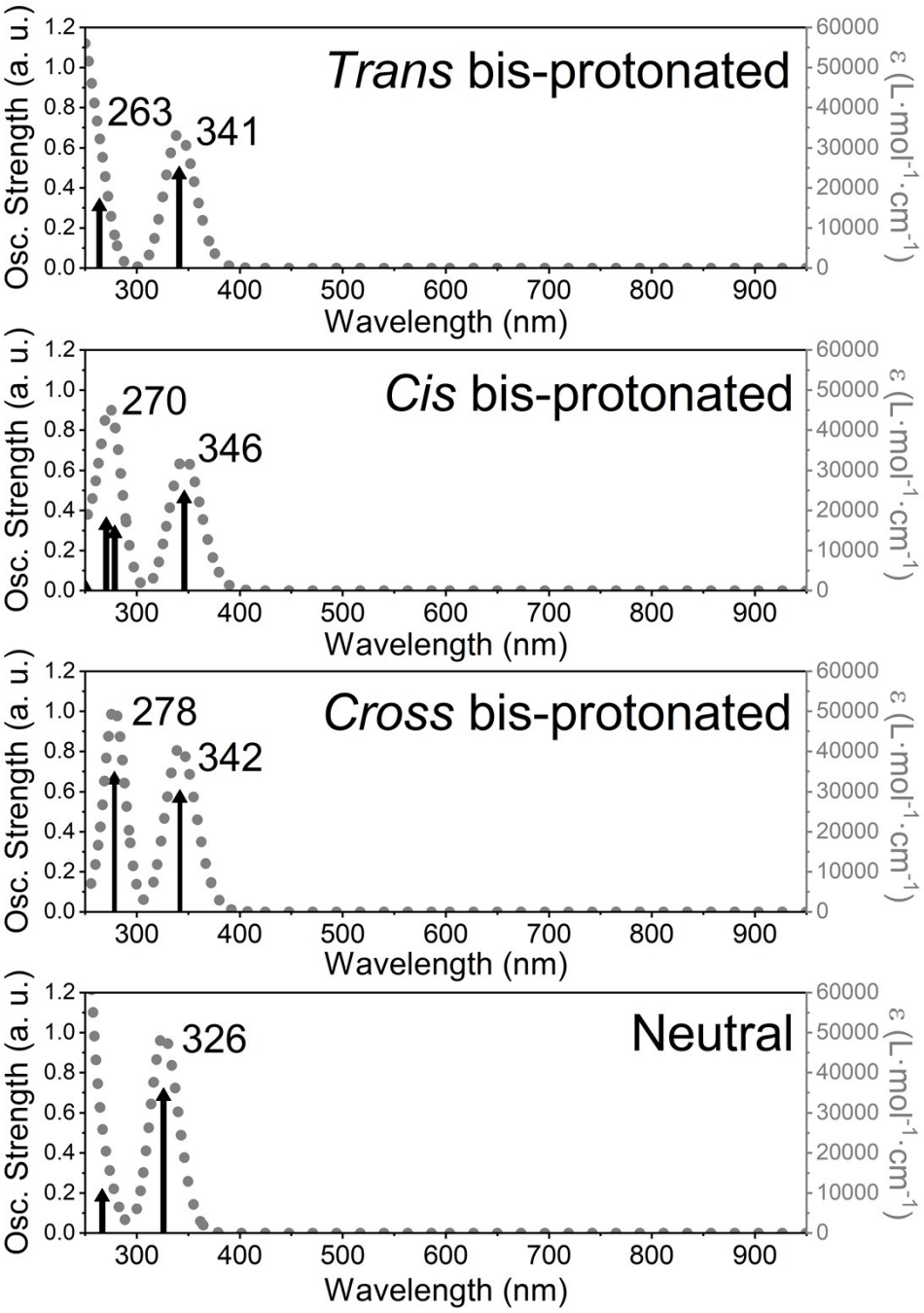

Figure S9. TD-DFT/CAM-B3LYP/6-31G** calculations in the framework of PCM model in CH_2Cl_2 of neutral and protonated species of **1**. From bottom to top: Neutral **1**; bisprotonated **1** in *cross* position; bisprotonated **1** in *cis* position; and bisprotonated **1** in *trans* position.

Table S1. Experimental and TD-DFT optical data of **1** upon protonation process.

	Experimental	TD-DFT		
		Vacuum B3LYP	PCM in CH_2Cl_2	
			B3LYP	CAM - B3LYP
Neutral	274 nm 340 nm	278 nm 380 nm	282 nm 388 nm	266 nm 326 nm
***cross*-Bisprotonated**	310-317 nm 436 nm	253 nm 436 nm 489 nm	258 nm 363 nm 421 nm	278 nm 342 nm
***cis*-Bisprotonated**		287 nm 328 nm 484 nm 691 nm	285 nm 358 nm 459 nm	270 nm 346 nm
***trans*-Bisprotonated**		307 nm 557 nm	300 nm 442 nm	263 nm 341 nm

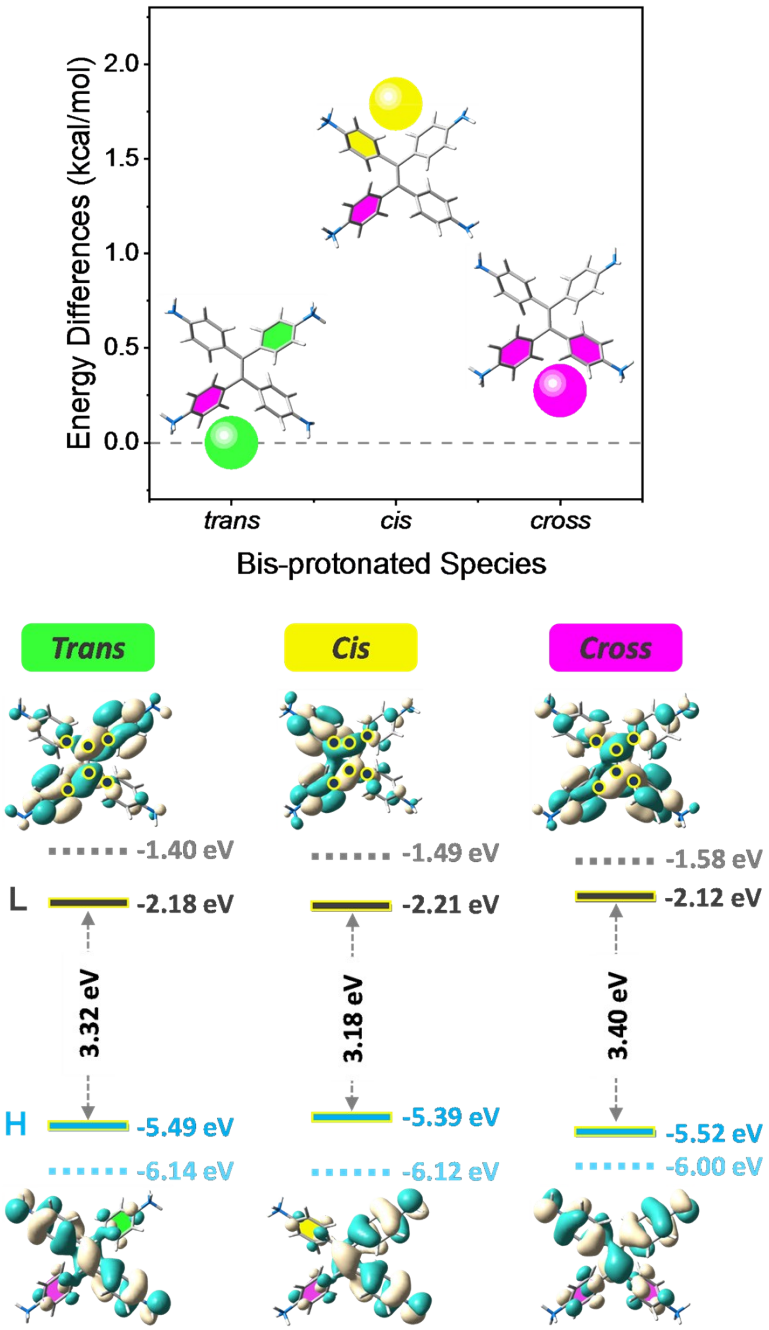

Figure S10. *Top*) Energy differences (in kcal/mol) of the *cis* (yellow circle) and the *cross* (pink circle) bisprotonated species of **1** respect to the *trans*-conjugated disposition (green circle) calculated at the B3LYP/6-31G** level of theory in the framework of PCM model in CH_2Cl_2, together with their corresponding optimized geometries; *Bottom*) Energy level diagram (in eV) of the frontier molecular orbitals of the *trans* (left), *cis* (middle) and *cross* (right) bisprotonated species of **1** calculated at the B3LYP/6-31G** level of theory in the framework of PCM model in CH_2Cl_2, together with the corresponding HOMO and LUMO topologies. Solid, blue lines correspond to the HOMO; grey solid lines correspond to the LUMO, and light blue and light grey dashed lines correspond to the HOMO-1 and LUMO-1, respectively.

The HOMO and LUMO of the three dications are shown in Figure S10 and their energies are indicated in Table S4. The HOMO energies vary in the range —5.4/—5.5 eV for the three species; however, in the *cis*- and *trans*- isomers their topologies reveal smaller atomic contributions along the paths between the protonated amino-benzene groups. Contrarily, the *cross*-conjugated dication displays larger atomic contribution along the inter-protonated path. For the LUMOs, lying in energy at —2.1/—2.2 eV, the situation is rather different since their main atomic contributions come from those atoms between the protonated amino groups thus favouring charge transmission in all cases.

Table S2. Energies (in kcal/mol) of the neutral and bisprotonated species of **1** with different DFT methodologies.

Energies (kcal/mol)	Vacuum B3LYP	PCM in CH_2Cl_2	
		B3LYP	CAM - B3LYP
Neutral	-768230.42461	-768242.68157	-767811.14856
***trans*-Bisprotonated**	-768658.25676	-768785.51487	-768351.8377
***cis*-Bisprotonated**	-768651.16636	-768783.72462	-768349.87676
***cross*-Bisprotonated**	-768656.49978	-768785.2394	-768351.27232
Triprotonated	-768798.81097	-769047.85003	-767811.14856

Table S3. Energy differences (in kcal/mol) between the *cis*-bisprotonated and the *cross*-bisprotonated species respect to the *trans*-bisprotonated **1** with different DFT methodologies.

ΔE (kcal/mol)	Vacuum B3LYP	PCM in CH_2Cl_2	
		B3LYP	CAM -B3LYP
cis-trans	7.09039	1.79026	1.96094
cross-trans	1.75697	0.27547	0.56538

Table S4. Energies of the frontier molecular orbitals and of the optical bandgap (in eV) of the bisprotonated species of **1** with different DFT methodologies.

	***trans*-Bisprotonated 1**		
	Vacuum B3LYP	**PCM in CH_2Cl_2**	
		B3LYP	**CAM - B3LYP**
LUMO+1	-5.73 eV	-1.40 eV	-0.08 eV
LUMO	-6.52 eV	-2.18 eV	-0.89 eV
HOMO	-9.20 eV	-5.49 eV	-6.81 eV
HOMO-1	-9.75 eV	-6.14 eV	-7.52 eV
E_g	**2.68 eV**	**3.32 eV**	**5.92 eV**
	***cis*-Bisprotonated 1**		
LUMO+1	-5.95 eV	-1.49 eV	-0.20 eV
LUMO	-6.66 eV	-2.21 eV	-0.90 eV
HOMO	-8.84 eV	-5.39 eV	-6.70 eV
HOMO-1	-9.51 eV	-6.12 eV	-7.50 eV
E_g	**2.18 eV**	**3.18 eV**	**5.80 eV**
	***cross*-Bisprotonated 1**		
LUMO+1	-6.04 eV	-1.58 eV	-0.29 eV
LUMO	-6.39 eV	-2.12 eV	-0.85 eV
HOMO	-9.25 eV	-5.52 eV	-6.81 eV
HOMO-1	-9.52 eV	-6.00 eV	-7.39 eV
E_g	**2.86 eV**	**3.40 eV**	**5.95 eV**

V. Single-Molecule Conductance Measurements

Single-molecule conductance measurements of **1** were performed using the scanning tunneling microscope break junction technique (STM-BJ)[15] as described previously.[16] In this technique, a gold tip is placed in proximity to a gold substrate in a solution of the analyte. Measurements herein were performed in 0.1 mM solutions in propylene carbonate. For each measurement, the gold tip is pressed into the substrate until a conductance of 5 G_0 is reached ($G_0 = 2e^2/h$). The tip is then retracted, allowing a small, atomically-defined gap to form between the tip and substrate. Molecule **1**, by means of the primary amines, can bridge this gap and form a single-molecule junction. The conductance (current/voltage) is recorded during the retraction, and a single-molecule junction manifests itself as a plateau-like feature below 1 G_0 in the conductance versus displacement trace. Several thousand conductance traces are recorded and plotted in logarithmically-binned one-dimensional (1D) conductance histograms (100 bins/decade) as well as two-dimensional (2D) histograms of conductance versus displacement.

VI. Transmission Calculations

The transmission calculations were performed using the Non-Equilibrium Green's Function (NEGF) method combined with DFT, as implemented in the Artaios code,[17, 18] a postprocessing tool for Gaussian 09. Gold(111) surfaces were chosen as electrodes and the amine groups were selected as anchor units to connect compound **1** to the contacts. Amine−gold molecular junctions were modeled according to the geometrical characteristics provided in the study of Venkataraman *et al.*[19] Amino anchor units bind to undercoordinated Au-adatoms located on top of the fcc-Au_9 clusters and the Au-N distance was set to 2.5 Å and the C-N-Au angle to 130°.[19] Previous calculations have shown that the conductance is relatively insensitive to amino-gold junction geometry.[19] The geometries of the molecular junctions for the *cis*-, *trans*- and cross-conjugated motifs are displayed in Figure S6. In order to assess the influence of the cluster size on the transport properties, the transmission calculations were performed considering three different Au clusters with varying size. Amino anchor units bind to undercoordinated Au-adatoms located on top of the fcc-Au_3, fcc-Au_9 and fcc-Au_{19} clusters (Figure S12).

In a next step, single-point calculations were performed at the B3LYP/LanL2DZ level of theory using the Gaussian 09 software. A previous study on iron porphyrin complexes showed that the transmission curves with B3LYP and B3P86 functionals are comparable and qualitative results are stable with respect to the functional used in the transmission calculations.[20]

The Hamiltonian and overlap matrices were extracted to carry out NEGF calculations within the wide-band-limit (WBL) approximation using the post-processing tool Artaios, which yield both transmission spectra and local transmission plots. In the WBL approximation, a constant value of 0.036 eV^{-1} for the local density of states of the electrode surface has been used. This value was taken from the literature.[21]

In our approach, which has been applied extensively in electron transport calculations,[22, 23, 24] the Fermi level is estimated to be located halfway between the HOMO and LUMO energy levels of the entire molecular junction (i.e. the molecule combined with the linkers and gold clusters on both sides). This is a reasonable approximation and appears to approach the experimental findings for the conductance in the literature.[25]

For production of the through-bond transmission plots, a threshold was set to 20% of the maximum atom-atom transmission calculated in order to better visualize the preferential

paths of the electrons through the different coordination modes to the gold electrodes. By setting such thresholds, i.e. by not drawing numerous (small) atom-atom contributions, the local transmission plots may falsely appear to not conserve the current.[26]

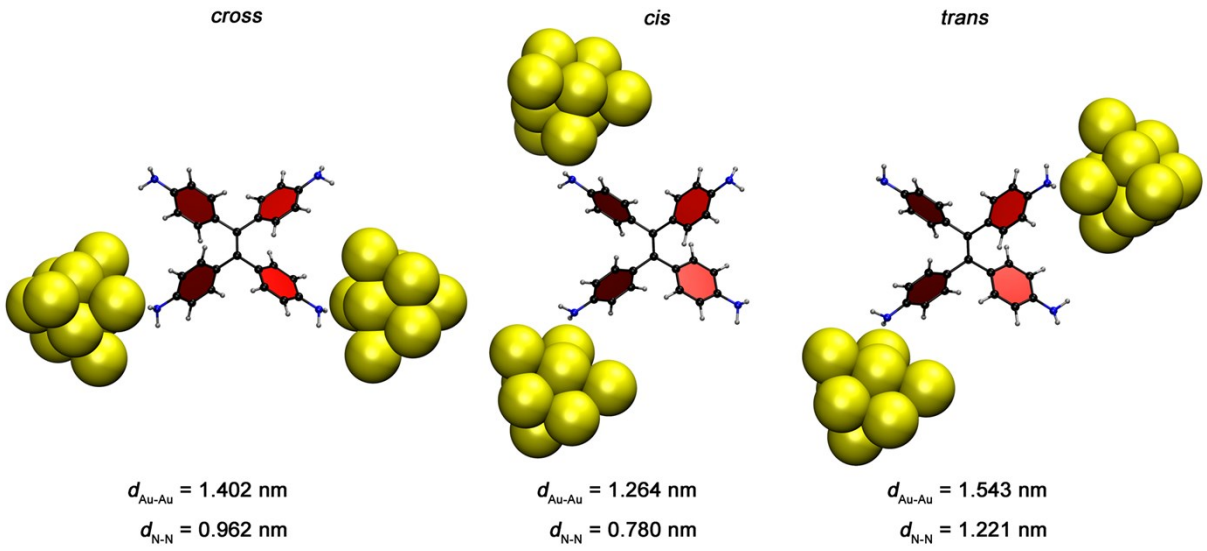

Figure S11. Structures of the molecular junctions for different connectivities of tetra-[(1,4)-aminobenzo]ethene **1** with the gold electrodes, corresponding to *cross*-, *cis*- and *trans*-anchoring modes. The Au-Au and N-N distances are also shown.

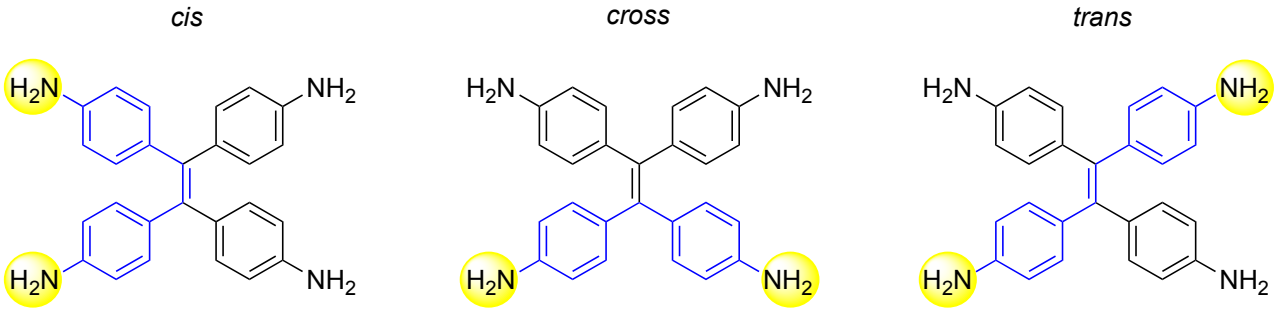

Figure S12. Different transmission paths (highlighted in blue) obtained for the *cis*-, *cross*- and *trans*-anchoring modes.

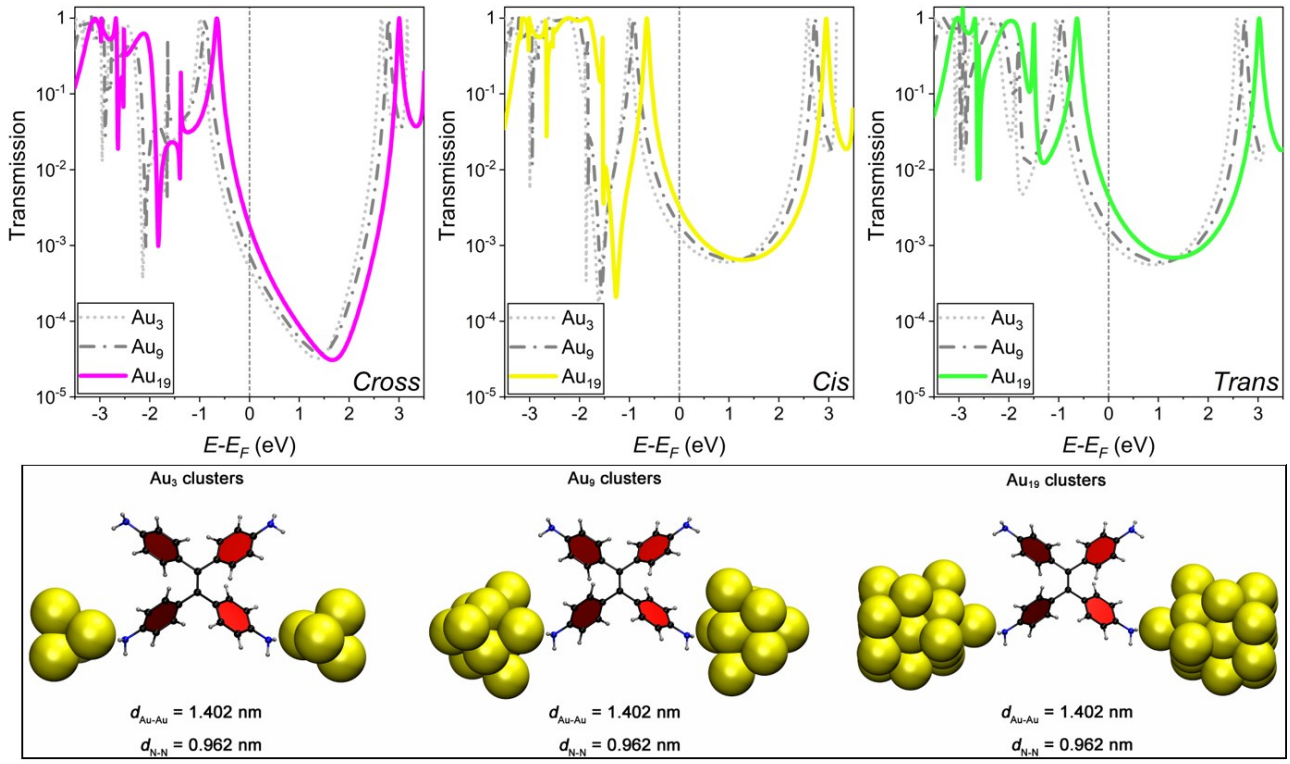

Figure S13. *Top*) Transmission spectra for the cross- (*left*), cis- (*middle*) and trans- (*right*) anchoring configurations of **1** on gold model cluster electrodes of 19, 9 and 3 atoms. *Bottom*) Structures of the molecular junctions for the three different gold cluster electrodes sizes in the *cross*-anchoring mode.

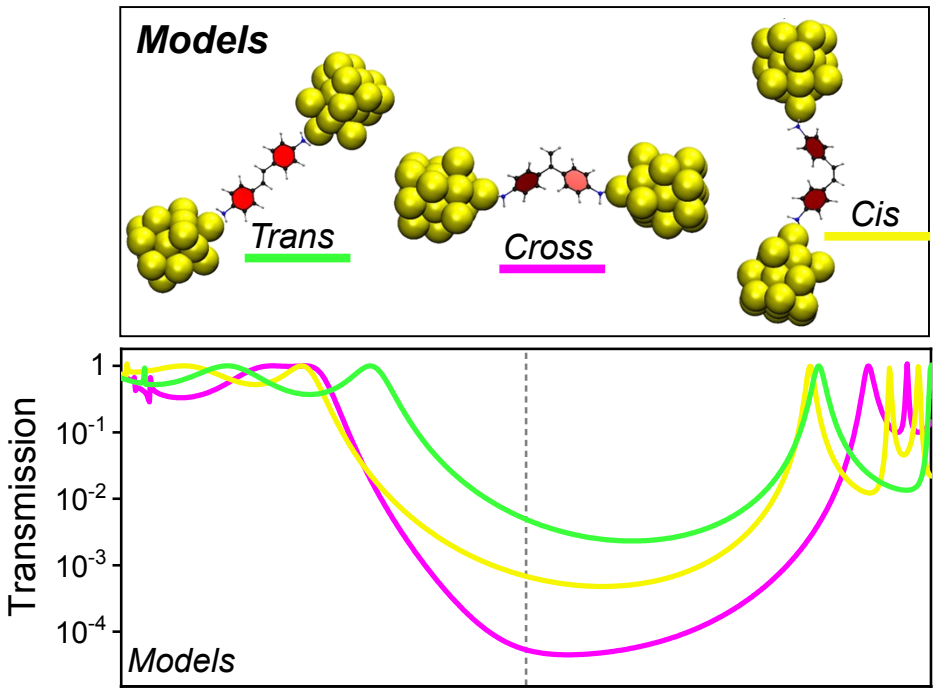

Figure S14. Theoretically predicted transmission spectra for the model-*cross*, model-*trans* and model-*cis* compounds anchored to Au_{19} cluster electrodes.

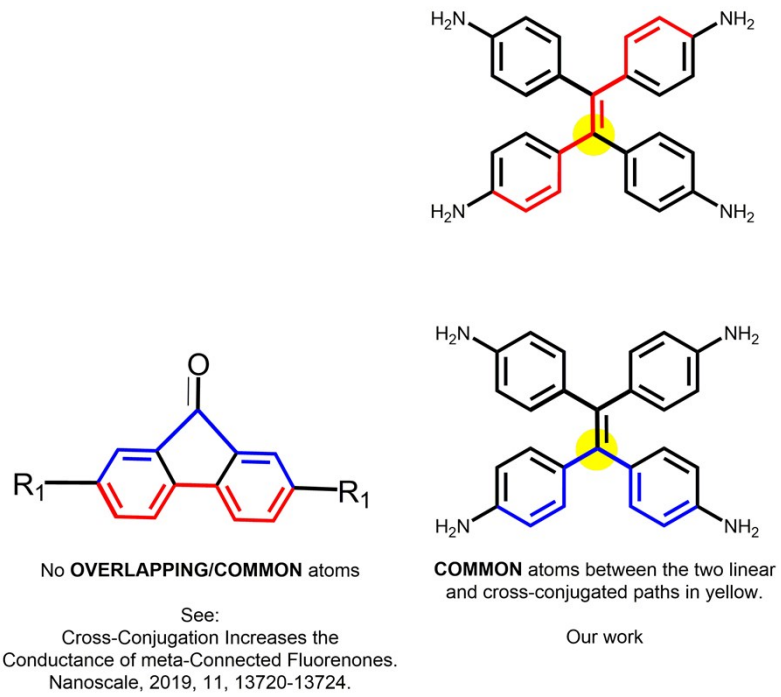

Figure S15. Comparison of cross-conjugated fluorenones and **1**.

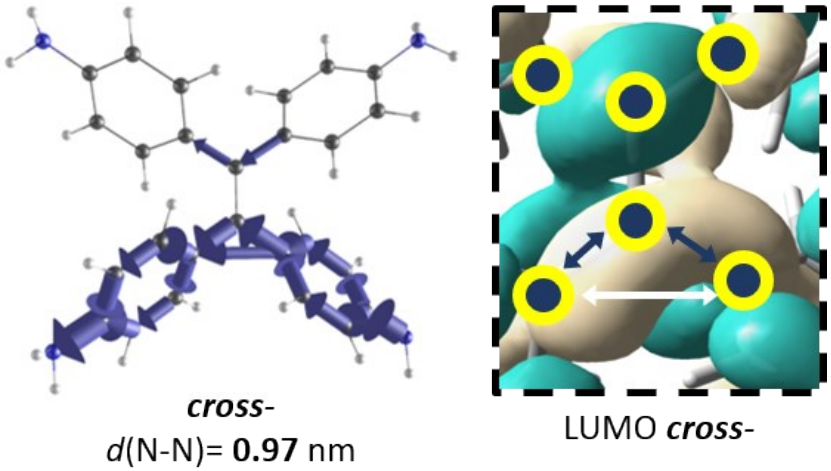

Figure S16. Local transmission plot at the Fermi level of the *cross*-conjugated geometry and the N-N distance for this transmission path. Zoom plot of the LUMO of the central molecular part of the *cross*-conjugated geometry with yellow circles showing the atoms, the white arrow showing the delocalization path between non-connected atoms and blue arrows displaying delocalization between connected atoms.

VII. References

[1] Y. Lin, X. Jiang, S. T. Kim, S. B. Alahakoon, X. Hou, Z. Zhang, C. M. Thompson, R. A. Smaldone, C. Ke, *J. Am. Chem. Soc.* **2017**, *139*, 7172–7175.

[2] T. Harder, P. Wessig, J. Bendig, R. Stösser, *J. Am. Chem. Soc.* **1999**, *121*, 6580–6588.

[3] X. Liu, H. Liu, W. Zhou, H. Zheng, X. Yin, Y. Li, Y. Guo, M. Zhu, C. Ouyang, D. Zhu, A. Xia, *Langmuir* **2010**, *26*, 3179–3185.

[4] G. J. Summers, M. P. Ndawuni, C. A. Summers, *Polym. Int.* **2014**, *63*, 876–886.

[5] Gaussian 16, Revision B.01, M. J. Frisch, G. W. Trucks, H. B. Schlegel, G. E. Scuseria, M. A. Robb, J. R. Cheeseman, G. Scalmani, V. Barone, G. A. Petersson, H. Nakatsuji, X. Li, M. Caricato, A. V. Marenich, J. Bloino, B. G. Janesko, R. Gomperts, B. Mennucci, H. P. Hratchian, J. V. Ortiz, A. F. Izmaylov, J. L. Sonnenberg, D. Williams-Young, F. Ding, F. Lipparini, F. Egidi, J. Goings, B. Peng, A. Petrone, T. Henderson, D. Ranasinghe, V. G. Zakrzewski, J. Gao, N. Rega, G. Zheng, W. Liang, M. Hada, M. Ehara, K. Toyota, R. Fukuda, J. Hasegawa, M. Ishida, T. Nakajima, Y. Honda, O. Kitao, H. Nakai, T. Vreven, K. Throssell, J. A., Jr. Montgomery, J. E. Peralta, F. Ogliaro, M. J. Bearpark, J. J. Heyd, E. N. Brothers, K. N. Kudin, V. N. Staroverov, T. A. Keith, R. Kobayashi, J. Normand, K. Raghavachari, A. P. Rendell, J. C. BurantS. S. Iyengar, J. Tomasi, M. Cossi, J. M. Millam, M. Klene, C. Adamo, R. Cammi, J. W. Ochterski, R. L. Martin, K. Morokuma, O. Farkas, J. B. Foresman, D. J. Fox, Gaussian, Inc., Wallingford CT, **2016**.

[6] A. D. Becke, *J. Chem. Phys*. **1993**, *98*, 1372–1377.

[7] M. M. Francl, W. J. Pietro, W. J. Hehre, J. S. Binkley, M. S. Gordon, D. J. Defrees, J. A. Pople, *J. Chem. Phys.* **1982**, *77*, 3654–3665.

[8] T. Yanai, D. Tew, and N. Handy, *Chem. Phys. Lett.* **2004**, *393*, 51–57.

[9] S. Miertus, E. Scrocco, J. Tomasi, *Chem. Phys.* **1981**, *55*, 117–129.

[10] S. Miertus, J. Tomasi, *Chem. Phys.* **1982**, *65*, 239–245.

[11] V. Barone, M. Cossi, and J. Tomasi, *J. Comp. Chem.* **1998**, *19*, 404–17.

[12] M. Cossi and V. Barone, *J. Chem. Phys.* **2001**, *115*, 4708–4717.

[13] R. E. Stratmann, G. E. Scuseria, and M. J. Frisch, *J. Chem. Phys.* **1998**, *109*, 8218–8224.

[14] G. Scalmani, M. J. Frisch, B. Mennucci, J. Tomasi, R. Cammi, and V. Barone, *J. Chem. Phys.* **2006**, *124*, 094107: 1-15.

[15] B. Q. Xu, N. J. J. Tao, *Science*, **2003**, *301*, 1221–1223.

[16] L. Venkataraman, J. E. Klare, C. Nuckolls, M. S. Hybertsen, M. L. Steigerwald, *Nature*, **2006**, *442*, 904–907.

[17] C. Herrmann, G. C. Solomon, J. E. Subotnik, V. Mujica, M. A. Ratner, *J. Chem. Phys.* **2010**, *132*, 024103.

[18] a) C. Hermann, L. Gross, T. Steenbock, G. C. Solomon, “Artaios – a code for postprocessing quantum chemical electronic structure calculations”, available from https://www.chemie.uni-hamburg.de/ac/herrmann/software/index.html (2008-2017).

[19] S. Y. Quek, L. Venkataraman, H. J. Choi, S. G. Louie, M. S. Hybertsen, J. B. Neaton, *Nano Lett.* **2007**, *7*, 3477-3482.

[20] C. Herrmann, G. C. Solomon, M. A. Ratner, *J. Phys. Chem. C* **2010**, *114*, 20813-

20820.

[21] C. Herrmann, G. C. Solomon, M. A. Ratner, *J. Chem. Phys.* **2011**, *134*, 224306.

[22] Y. Tsuji, R. Hoffmann, R. Movassagh, S. Datta, *J. Chem. Phys.* **2014**, *141*, 224311.

[23] M. H. Garner, G. C. Solomon, M. Strange, *J. Phys. Chem. C* **2016**, *120*, 9097-9103.

[24] T. Stuyver, M. Perrin, P. Geerlings, F. De Proft, M. Alonso, *J. Am. Chem. Soc.* **2018**, *140*, 1313-1326.

[25] Y. Tsuji, R. Hoffmann, *Angew. Chem. Int. Ed.* **2014**, *53*, 4093-4097.

[26] G. C. Solomon, C. Herrmann, T. Hansen, V. Mujica, M. A. Ratner, *Nat. Chem.* **2010**, *2*, 223-228.